



ARTICLE

Folic Acid-Functionalized Nanocrystalline Cellulose as a Renewable and Biocompatible Nanomaterial for Cancer-Targeting Nanoparticles

Thean Heng Tan¹, Najihah Mohd Hashim², Wageeh Abdulhadi Yehya Dabdawb¹, Mochamad Zakki Fahmi^{3,*} and Hwei Voon Lee^{1,*}

¹Nanotechnology & Catalysis Research Center (NANOCAT), Universiti Malaya, Kuala Lumpur, 50603, Malaysia

²Department of Pharmaceutical Chemistry, Faculty of Pharmacy, Universiti Malaya, Kuala Lumpur, 50603, Malaysia

³Department of Chemistry, Faculty of Science and Technology, Universitas Airlangga, Campus C, Mulyorejo, Surabaya, 60115, Indonesia

*Corresponding Authors: Mochamad Zakki Fahmi. Email: m.zakki.fahmi@fst.unair.ac.id; Hwei Voon Lee. Email: leehweivoon@um.edu.my

Received: 03 July 2023 Accepted: 30 August 2023 Published: 23 January 2024

ABSTRACT

The study focuses on the development of biocompatible and stable FA-functionalized nanocrystalline cellulose (NCC) as a potential drug delivery system for targeting folate receptor-positive cancer cells. The FA-functionalized NCCs were synthesized through a series of chemical reactions, resulting in nanoparticles with favorable properties for biomedical applications. The microstructural analysis revealed that the functionalized NCCs maintained their rod-shaped morphology and displayed hydrodynamic diameters suitable for evading the mononuclear phagocytic system while being large enough to target tumor tissues. Importantly, these nanoparticles possessed a negative surface charge, enhancing their stability and repelling potential aggregation. The binding specificity of FA-functionalized NCCs to folate receptor-positive cancer cells was demonstrated through various assays. The free folic acid inhibition assay showed approximately 30% decrease in the binding of functionalized NCCs in the presence of just 5 mM free FA, confirming their selectivity for folate receptor-positive cells. Confocal microscopy further validated this specificity, as only cancer cells displayed significant binding of functionalized NCCs. Crucially, biocompatibility tests revealed that both NCCs and FA-functionalized NCCs had minimal effects on red blood cells, and they did not induce erythrocyte aggregation. Furthermore, cell viability assays demonstrated functionalized NCCs have selective cytotoxicity against colorectal cancer cells HT-29 and SW-620 (68%–88% cell viability) while sparing noncancerous colon cells CCD-18Co (81%–97% cell viability). In summary, FA-functionalized NCCs exhibit promising characteristics for targeted drug delivery in cancer therapy. Their biocompatibility, stability, and selective cytotoxicity make them an attractive option for delivering therapeutic agents to folate receptor-positive cancer cells, potentially improving the effectiveness of cancer treatments while minimizing harm to healthy tissues.

KEYWORDS

Agricultural wastes; sustainable nanocarrier; blood biocompatibility; folic acid receptor; drug delivery system; nanomedicine



1 Introduction

Over the past few years, there has been a growing interest in natural polymers sourced from renewable biomass resources, such as cellulose, as they offer numerous advantages like affordability, recyclability, and biodegradability [1–3]. Continuous population growth and industrialization resulted in a high abundance of agricultural residues, which present a valuable opportunity for the upgrading of waste into cellulose with nano aspects, which offers a promising avenue for advancing sustainability and creating innovative solutions across multiple industries. The conversion of agricultural waste into nano-based biomaterials for biomedical applications presents an innovative and sustainable approach in the field of healthcare. Agricultural residues and by-products can be utilized to create biomaterials with diverse functionalities, such as wound dressings, drug delivery systems, tissue engineering scaffolds, and bioactive compounds [4–6].

Particularly, cellulose in nano-dimension like bacterial cellulose [7], cellulose nanofibers (CNF) [8], and nanocrystalline cellulose [9] (NCC) were developed for biomedical applications. NCC in particular, possesses a unique combination of characteristics that make it a promising nanocarrier for cancer cell targeting agents in biomedical and therapeutic treatment. Some of these properties include being highly biocompatible with the biological system; large surface area enables a wide range of surface functionalization with targeting ligands for selective binding cancer-targeting cells; controllable of nanosized and nanostructures for optimal cellular uptake and targeting; excellent stability ensures the loaded drugs or targeting agents remain protected and intact during storage and transportation; controlled drug release properties for optimal drug concentration release at the targeted cancer site [10]. Thus, NCC has surpassed those of regular cellulose, thereby making it extremely suitable as a renewable nanocarrier for biomedical applications and drug delivery systems [11,12].

NCC stands out as a superior nanomaterial compared to other nanomaterials in biomedical applications. When compared to carbon nanotubes (CNTs), nanocellulose exhibits exceptional biocompatibility, ensuring minimal adverse reactions when in contact with living systems. Carbon nanotubes, while possessing unique properties such as high mechanical strength and electrical conductivity, raise concerns regarding cytotoxicity and long-term biocompatibility [13]. Similarly, nanocellulose surpasses graphene in terms of biocompatibility and biodegradability. Graphene offers remarkable electrical and mechanical properties, but its cytotoxicity and potential accumulation in the body raise concerns for long-term biomedical usage. In contrast, nanocellulose, being a naturally derived material, is biocompatible and biodegradable, making it a safer choice for biomedical applications [14]. In addition, NCC potentially outshines metal nanoparticles (e.g., gold or silver) in biomedical applications, due to its enhanced biocompatibility and ease of functionalization. While metal nanoparticles may exhibit antimicrobial or optical properties, however, their potential toxicity and limited surface modifications restrict their use in biomedical applications [15]. Furthermore, NCC offers an alternative to lipid-based nanoparticles. Lipid nanoparticles are commonly used for drug encapsulation and delivery, but they may face challenges related to stability and limited cargo capacity as compared to NCC [16].

Developing cancer-targeting nanoparticles will involve either active targeting, which is based on ligand affinity to the receptor, or passive targeting, which is based on enhanced permeability and retention effect [17]. In the selection of a suitable receptor for cancer-targeting nanoparticles, it is crucial to consider various criteria, with the primary focus on the substantial over-expression of the specific receptor on cancerous tissues in comparison to normal cells. One such receptor family that satisfies these criteria is the folate receptors, which are glycoproteins with a molecular weight of 35-40 kDa [18]. Folate receptors (known as vitamin B9) mediate cellular uptake of folic acid (FA), are overexpressed on the plasma membrane of many cancer cell types, including breast [19], endometrial [20], ovarian [21], and central nervous system [22] cancer. Meanwhile, normal tissues rarely express folate receptors [23,24]. Thus, folate receptors are of particular interest in cancer research because they are often overexpressed on the

plasma membrane of cancer cells, making them a potential cancer-targeting agent for cancer therapies and diagnostic approaches.

Thus, the present study focuses on the development of novel, cost-effective FA-functionalized nanocrystalline cellulose to target tumor cancer that is folate receptor positive. The FA-functionalized NCCs were synthesized by functionalizing folic acid (FA) to nanocrystalline cellulose (NCC) as nanocarriers via the amino-acylation reaction. The micro-structural properties of both NCC and FA-functionalized NCCs were determined through several analyses (e.g., particle size distribution and chemical surface functional analysis). Subsequently, the cancer-targeting specificity of FA-functionalized NCCs was determined using HT-29 and SW-620 cancer cells. Meanwhile, CCD-18Co cells will be used as a negative control as a comparison. Blood biocompatibility was also tested using human blood samples.

2 Materials and Methods

2.1 Surface Functionalization of NCC

Nanocrystalline cellulose (NCC) was prepared from agricultural residues according to our group studies [25–27]. Fluorescein isothiocyanate (FITC), Folic acid (FA), 1-chloro-2,3-epoxypropane (epichlorohydrin), N-(3-Dimethylaminopropyl)-N'-ethylcarbodiimide hydrochloride (EDC) and N-hydroxysulfosuccinimide (sulfo-NHS) was purchased from Sigma-Aldrich. The functionalization process of NCC was conducted by treating the surface-OH groups with a mixture of NaOH (50% w/v) and an excess of epichlorohydrin. The resulting mixture was then poured into dialysis tubing and subjected to dialysis using deionized water. Once the pH of the NCC mixture reached a value below 12, the epoxy-activated NCCs suspension was poured into a flask. A surplus of aqueous NH_4OH (28.7%) is introduced to the reaction mixture. The mixture was then poured back into dialysis tubing and subjected to dialysis using deionized water. Dialysis was halted when the pH inside the tubing remained stable, and the suspension was subjected to sonication under ice-bath cooling for 10 min at 40% output. Subsequently, the NCC- NH_2 suspension was centrifuged at 6000 RPM for 10 minutes, and the sediment was discarded. The concentration of the resulting aqueous suspension of NCC- NH_2 was determined using gravimetric analysis and subsequently increased for the subsequent reaction by employing rotary evaporation [28].

In this study, FITC (fluorescein isothiocyanate) is employed as a crucial fluorescence tag for the investigation of NCC. FITC is chosen for its exceptional fluorescence properties, high quantum yield, and compatibility with a wide range of biological and material systems. By conjugating FITC to NCC, we can impart a fluorescent signal that enables the visualization and tracking of NCC in complex biological environments. The bright green fluorescence emitted by FITC serves as a powerful tool for fluorescence imaging and quantification, allowing real-time monitoring of nanoparticle behaviour and distribution [29,30]. FITC was chemically attached into aminated NCC (NCC- NH_2) by reacting with the isothiocyanate group of FITC to form thiourea. This was carried out by adding FITC into a stirring flask containing NCC- NH_2 in a buffer solution covered in aluminium foil to prevent exposure to light. The solution was left overnight in the dark for the reaction to continue. The reaction mixture was dialyzed until dialysis water showed no FITC UV-vis readings. FITC-NCC was harvested by centrifuging it for 10 min at 6000 RPM [31].

Folic acid (FA) was chemically functionalized to both FITC-NCC and NCC- NH_2 (0.1 wt%) with N-(3-Dimethylaminopropyl)-N'-ethylcarbodiimide hydrochloride (EDC) and N-hydroxysulfosuccinimide (sulfo-NHS) to yield FA-functionalized NCCs (denoted as FTIC-NCC-FA and NCC-FA), respectively. The reaction was conducted under stirring in the dark at room temperature for a duration of 40 h. The resulting reaction mixture was then processed using the methods previously described, including dialysis, sonication, centrifugation, and subsequent dialysis.

2.2 Microstructural Analysis of FA-Functionalized NCCs

The functional groups present in native cellulose and nanocellulose obtained through hydrolysis treatment were examined using Fourier transform-infrared spectroscopy (FTIR). The FTIR analysis was conducted using a Bruker IFX 66/S FTIR spectrometer (PerkinElmer, Germany) to investigate the chemical composition changes induced by the hydrolysis treatment. Transmittance mode was employed for the FTIR analysis, covering a wavelength range of 4000–400 cm^{-1} with a resolution of 4 cm^{-1} and averaging 32 scans. Prior to analysis, the samples were ground and mixed with KBr powder in a ratio of 1:100 (w/w). Subsequently, the mixture was pressed into an ultra-thin pellet for analysis.

Triplicate of ζ -potentials was measured with the Zetasizer Nanoseries ZS (Malvern, UK). The samples were analyzed under 25°C without the addition of electrolyte. Samples were sonicated for 10 min with the final concentration of 0.01 wt%.

Triplicate of dynamic light scattering (DLS) was measured with the Zetasizer Nanoseries ZS (Malvern, UK). Samples were sonicated for 10 min with the final concentration of 0.01 wt% and measured in 12 mm square glass cuvettes (Malvern PCS 1115). Samples were filtered using a 0.45 μm poly(vinylidene fluoride) syringe filter.

The size and dimensions of yielded nanocellulose were investigated by a transmission electron microscope (TEM), as described previously [25]. The morphology and diameter of the yielded nanocellulose fibers were determined by analyzing the micrographs with ImageJ software (National Institutes of Health, New York, NY, USA).

2.3 Study of Cancer Cells for Binding with FA-Functionalized NCCs

HT-29 and SW-620 were selected for FA binding study as both are folate receptor positive cancer cell lines that show high binding affinity towards FA [32,33]. The HT-29 and SW620 cell lines were purchased from the American Type Culture Collection (ATCC, Rockville, MD, USA). Both HT-29 and SW 620 cells were cultured using DMEM with 10% of heat-inactivated fetal bovine serum and penicillin/streptomycin (100 units/mL of penicillin and 100 $\mu\text{g}/\text{mL}$ of streptomycin) in a humidified incubator with 5% CO_2 atmosphere at 37°C. Cells in 96-well plates were incubated with FITC-NCC-FA at a FITC concentration of 5 $\mu\text{g}/\text{mL}$ in the presence of 0, 5, 10, or 25 mM FA for 2 h. The FA binding capacity of cells was then analyzed using a SpectraMax M5 plate reader (Molecular Devices, Sunnyvale, CA, USA) with excitation and emission wavelengths of 485 and 520 nm, respectively.

Confocal Laser Scanning Microscopy (CLSM) analysis was further conducted on both cells by removing the inoculum from the flasks and washing the cell monolayers three times with PBS. The cells were trypsinized and treated for 6 h with FITC-NCC-FA followed by treatment with Alexa Fluor 594 (a cell membrane-specific dye). The cells were transferred to slides and fixed with 99% ethanol for 10 min at 4°C and air dried. Slides were analyzed with Fluoview 300 confocal laser scanning microscope (Olympus America) at a magnification of 6400 and Fluoview software.

2.4 Biocompatibility Tests

The human blood sample was obtained from Innovative Research (Novi, MI, USA). The blood sample underwent centrifugation at 700 g and 4°C for 10 min, followed by multiple washes with PBS until the supernatant became colourless. A 500 μL portion of a 2.5% (v/v) suspension of erythrocytes was combined with 500 μL of a polymer solution in Eppendorf cups. The mixture was then incubated at 37°C in a shaking water bath for 2 and 60 min. After centrifugation, the blood cells were separated, and the resulting supernatants were analyzed spectroscopically at 540 nm to assess the release of haemoglobin. PBS (negative = 0%) and a 0.2% Triton X-100 solution (positive = 100%) were used as reference [34]. The experiments were performed in triplicate.

In order to investigate the aggregation of erythrocytes induced by nanoparticles, the human blood sample was utilized. To prevent coagulation, a pH of 7.4 was maintained in Ringer's solution by adding sodium citrate as a supplement. The blood sample was washed multiple times with Ringer's solution until the supernatant became colourless. Subsequently, the erythrocytes were diluted 50-fold with Ringer's solution. The negative control consisted of incubating the cells solely with Ringer's solution, while the modified negative control excluded sodium citrate from Ringer's solution. In 24-well plates, 200 μL of the cell suspension was mixed with 100 μL of a nanoparticle-containing solution. Following a 2-h incubation period at 37°C, images of the cells were captured using a Nikon Coolpix 885 camera with a microscope adapter attached to a reverse phase contrast microscopy setup (Nikon TMS) at 40x magnification [34]. The experiments were conducted in triplicate.

2.5 Cell Toxicity Test

For cell toxicity tests, HT-29, SW-620 and CCD-18Co cell lines were used. CCD-18Co is a human fibroblast cell line isolated from normal colon tissue. The cell line was purchased from the American Type Culture Collection (ATCC, Rockville, MD, USA). CCD-18Co was cultured in complete growth media consisting of: high-glucose (4.5 g/L) DMEM supplemented with 10% heat-inactivated FCS, 0.1 mM non-essential amino acids, 2 μM L-glutamine, 100 units/mL penicillin and 100 units/mL streptomycin in a humidified incubator with 5% CO₂ atmosphere at 37°C and maintained in T-225 flasks. A fixed number of cells was added into each well of a 96-well microplate provided with 200 μL of culture medium. Then, the cells are treated with varying concentrations of NCC, NCC-FA and FITC-NCC-FA. Then the cells were incubated for 24 h. Thereafter, cell viability is examined after 24 h using an MTT assay for the cell toxicity test.

2.6 Statistical Analysis

All experiments and measurements were performed in triplicate or three trials. The results were expressed as means of the standard deviation (SD).

3 Results and Discussion

3.1 Microstructural Properties of FA-Functionalized NCCs

Fig. 1 displays the FTIR spectra of various samples, including non-functionalized NCC, aminated NCC (NCC-NH₂), FITC, FITC-NCC, FA, and FITC-NCC-FA. Notably, the FTIR spectra of non-functionalized NCC (Fig. 1i) and NCC-NH₂ (Fig. 1iii) exhibited minimal differences, primarily because the absorption bands corresponding to the additional functional groups (OH, NH₂, and CH₂) in NCC-NH₂ were overshadowed by the broader cellulose-related OH- and CH-stretching bands at 3200–3600 cm^{-1} and 2900 cm^{-1} , respectively [35]. The FTIR spectrum of FITC-NCC (Fig. 1iv) revealed an additional absorption band around 1600 cm^{-1} , indicating the C=O stretching vibration of protonated FITC carboxyl groups. Notably, the FITC spectrum (Fig. 1iii) displayed a prominent band in the range of 2000–2200 cm^{-1} , which was absent in the FITC-NCC spectrum. This FTIR band in the FITC spectrum originated from the asymmetric stretching vibration of the isothiocyanate group (N=C=S). During the coupling reaction, this isothiocyanate group was transformed into a thiourea group (NH-C(=S)-NH), which does not exhibit a distinct band in the FITC-NCC spectrum. Thus, the absence of this band in the FITC-NCC spectrum provides evidence for the covalent attachment of FITC moieties to the NCCs. The absorption band corresponding to the formed thiourea group is found around 1550 cm^{-1} , which coincides with the FITC COOH band in the FITC-NCC spectrum, leading to its overlap [36]. The FTIR spectrum of FITC-NCC-FA (Fig. 1vi) exhibits several distinct bands that correspond to various chemical groups present in FA (Fig. 1v). Notably, the most prominent bands observed in the spectrum range between 1570 and 1700 cm^{-1} , which can be attributed to the carboxyl and amide groups [37]. The presence of both FITC and FA moieties in FITC-NCC-FA is indicated by the ratio of absorption intensities at

1600 and 1690 cm^{-1} (amide I) [37]. From the spectrum of FA, the absorption intensities at 1600 and 1690 cm^{-1} are approximately equal. However, the intensity of the band at 1600 cm^{-1} is higher than that at 1690 cm^{-1} for FITC-NCC-FA. This is because the absorption at 1600 cm^{-1} is contributed by the carboxyl groups present in both FITC and FA.

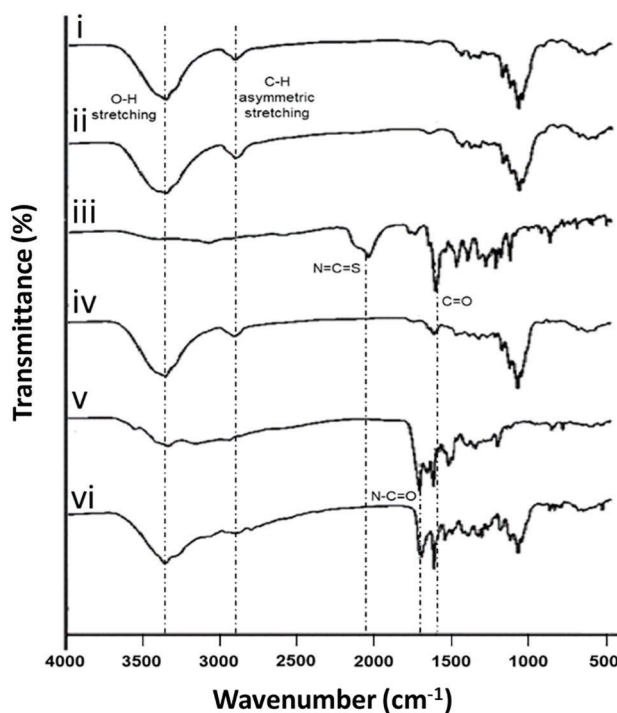


Figure 1: FTIR absorption spectra of (i) non-functionalized NCC, (ii) NCC-NH₂, (iii) FITC, (iv) FITC-NCC, (v) FA, and (vi) FITC-NCC-FA

Particle size distribution of functionalized NCCs by using Transmission Electron Microscopy (TEM) analysis showed that the width and length of FITC-NCC and FITC-NCC-FA were larger as compared to non-functionalized NCCs (Fig. 2). However, TEM images confirmed that both functionalized NCCs able to retain the rod-shapes of nanocrystallites (Figs. 2i–2iii). One crucial aspect of tumor-targeting nanoparticles is their ability to be tailored in size. Thus, it is crucial to strike a balance in designing nanoparticles, where they are large enough to prevent rapid penetration into fenestrated blood vessels, yet small enough to evade phagocytosis by macrophages found in the reticuloendothelial system, such as the liver and spleen. The fenestrae size of Kupffer cells in the liver and sinusoids in the spleen typically range from 150 to 200 nm [38]. While the size of fenestrae between endothelial cells in the fenestrated tumor vasculature can vary between 100 and 600 nm [39]. Therefore, nanoparticles should have a size of up to 100 nm to effectively reach tumor tissues by traversing these specific vascular structures while evading the macrophages. In the case of nanocellulose, its lateral measurements range from 10 to 40 nm (Figs. 2iv–2vi), while the longitudinal dimension spans from 20 to 100 nm (Figs. 2vii–2ix). Thus, the synthesized NCC meets the necessary size criteria for a drug delivery system targeting tumor sites. The prepared NCCs and functionalized NCCs consisted of dimensions that are sufficiently small to evade the mononuclear phagocytic system, yet it is too large to be rapidly cleared through renal excretion [40]. In contrast, NCC is anticipated to align with the blood flow direction and eventually traverse the fenestrations in the kidney's glomeruli, facilitating its eventual excretion in the urine owing to its unique rod-shape network as shown in Figs. 2i–2iii [41].

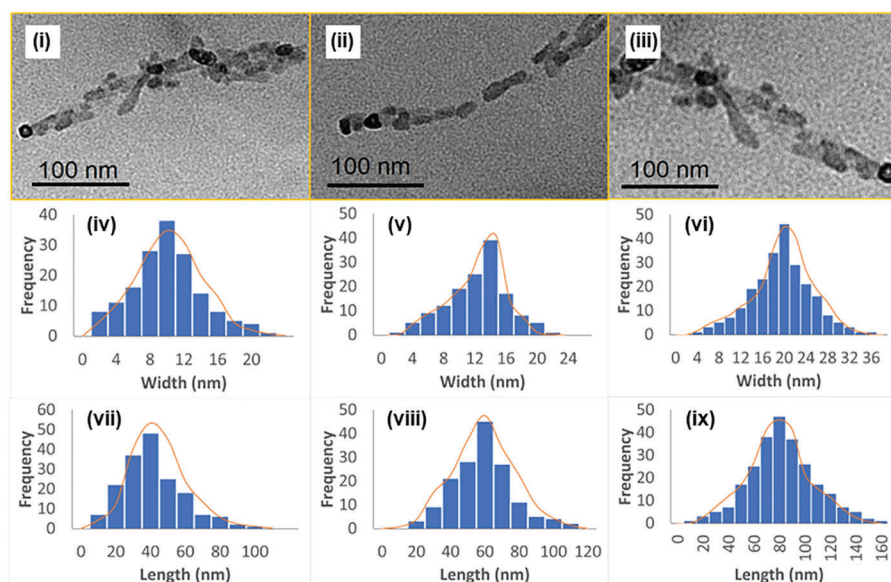


Figure 2: TEM profile of NCC (i), FITC-NCC (ii), and FITC-NCC-FA (iii); Histograms of TEM width data (iv–vi); and Histograms of TEM length data (vii–ix) with the skew normal fits shown as orange lines

The surface charge of nanoparticles can profoundly impact their interaction with biological systems. ζ -potential analysis showed non-functionalized NCCs had a negative particle surface charge, which indicated a stable NCC suspension with repulsive force to prevent particle aggregation and agglomeration (Table 1) [42,43]. This could potentially lead to improved accumulation at the target site. Even after functionalization, both FITC-NCC and FITC-NCC-FA retained their negative particle surface charge. Results from DLS showed that the hydrodynamic diameters of FITC-NCC and FITC-NCC-FA were larger than that of nonfunctionalized NCCs. However, TEM images confirmed that both FITC-NCC and FITC-NCC-FA still had the initial rod-shaped particles.

Table 1: Hydrodynamic diameter and ζ -potential of NCCs and functionalized NCCs

Samples	Hydrodynamic diameter		ζ -potential (mV) ^a
	(nm) ^a	(PDI) ^b	
NCCs	42 ± 8	0.31	-45 ± 3
FITC-NCC	69 ± 16	0.33	-41 ± 2
FITC-NCC-FA	94 ± 23	0.32	-43 ± 5

Note: ^aData shown are means ± standard deviations. ^bPDI: polydispersity index.

3.2 Folic Binding Profile of FA-Functionalized NCCs

The binding capacity of FITC-NCC-FA with folate receptor was determined through free folic inhibition assay. Both HT-29 and SW-620 cells were incubated with FITC-NCC-FA with different concentrations of free FA (0–25 mM). As the free FA concentration increased to 25 mM, the amount of FITC-NCC-FA binding to cells was decreased (Fig. 3). The decrease in FITC-NCC-FA binding/uptake in the presence of free FA implies that FITC-NCC-FA uptake by folate receptor-negative cells will be minimal, implying that FITC-NCC-FA is selective for folate receptor-positive cells. Various research revealed a substantial decrease in FA functionalized NCCs binding even at free FA concentrations of 1 mM or less [44,45]. From this study,

with just 5 mM of free FA, a reduction of approximately 30% was observed for both HT-29 and SW-620 cells. According to Leamon et al. [46], folate receptor-mediated endocytosis is heavily affected by the steric environment around the FA's p-aminobenzoic acid moiety. So, the p-aminobenzoic acid moiety of the FA-functionalized NCCs could influence their cellular uptake efficiency. From the results of the high binding affinity of FA-functionalized NCCs, a low concentration of the functionalized nanoparticles will be sufficient to achieve considerable cellular uptake if it is used in biomedical applications. This effect could also subsequently impact the therapeutic payload delivery to the targeted cancer cells.

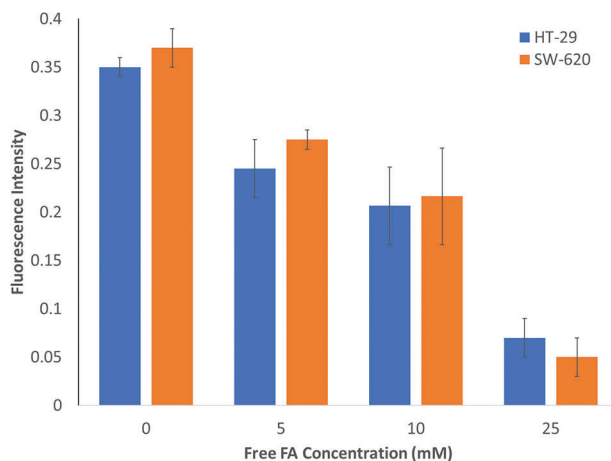


Figure 3: Effects of free FA on cellular binding of FITC-NCC-FA by HT-29 and SW-620 cells. Cells were exposed to FITC-NCC-FA and increasing concentrations of FA for 2 h

To further validate FA receptor targeting specificity of functionalized NCCs, HT-29 (A) and SW-620 (B) cells were observed under confocal laser scanning microscope after incubated in free FITC, FITC-NCC and FITC-NCC-FA (Fig. 4). CCD-18Co (C) cells were used as a negative control for folate receptors. FITC and FITC-NCC were used as negative control because there was no FA present to bind to the cells' folate receptors (ii, vi). HT-29 (A) and SW-620 (B) cells incubated with nontargeted free FITC (i–iv) or FITC-NCC (v–viii) show little to no binding. Meanwhile, cells incubated with folate receptor targeting FITC-NCC-FA (ix–xii) showed significant binding of the nanoparticles. As expected, when FITC-NCC-FA (ix–xii) was incubated with CCD-18Co (C), there was no binding observed under the confocal laser scanning microscope.

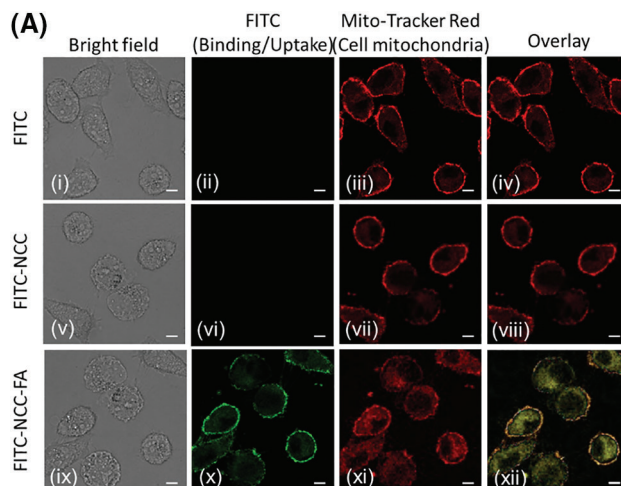


Figure 4: (Continued)

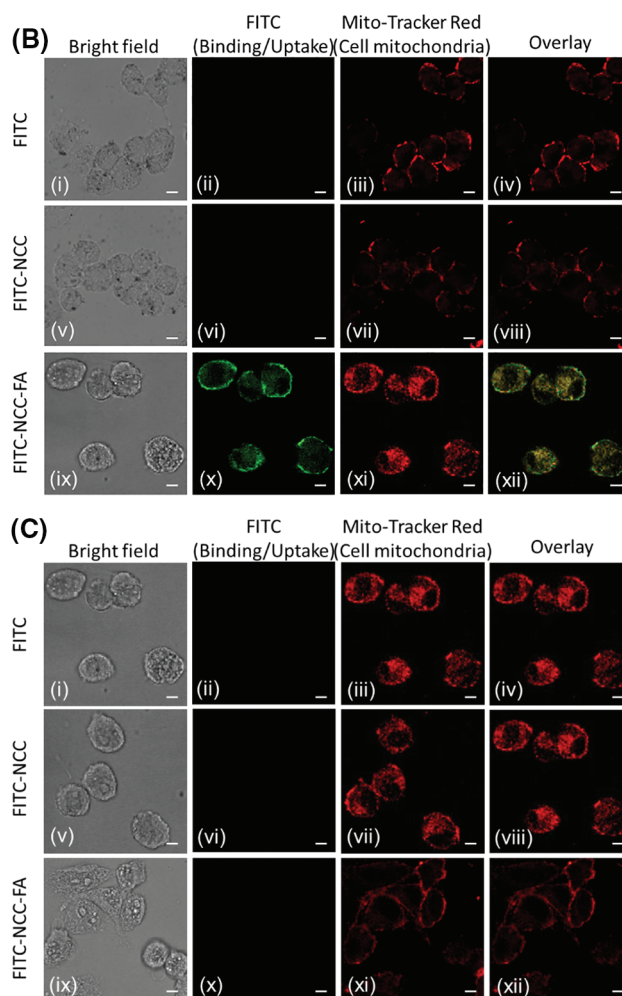


Figure 4: Cellular binding of free FITC (i–iv), FITC-NCC (v–viii), and FITC-NCC-FA (ix–xii). HT-29 (A), SW-620 (B) and CCD-18Co (C) cells were exposed to either free FITC, FITC-NCC or FITC-NCC-FA for 2 hours, stained with Alexa Fluor 594. The images were achieved by confocal microscopy. Images shown in (A) and (B) represent cells in bright field (i, v, ix), bound nanoparticles (ii, vi, x), cell membrane (iii, vii, xi), and overlay images of each group (iv, viii, xii). Bar: 10 μ m

3.3 Biocompatibility Tests

In haemolysis test (Fig. 5), the percentage of red blood cell lysis in all samples treated with NCC and NCC-FA was minimal (<3%). There was no significant difference between samples treated with NCC and NCC-FA compared to negative control ($p > 0.05$ for all comparisons). In contrast, samples treated with NCC and NCC-FA were significantly lower compared to positive control ($p < 0.05$). In the red blood cell aggregation test (Fig. 6), red blood cell aggregation was not observed in all samples treated with NCC and NCC-FA. In contrast, signs of red blood cell aggregation were evident in the positive control. From the haemocompatibility tests, it was proven that NCC and NCC-FA were blood compatible. The low percentage of red blood cell lysis (<3%) in negative control and samples treated with NCC and NCC-FA was most likely the side effect of mechanical stress induced by experimental procedures such as pipetting and centrifuging. Numerous studies also showed NCC to be of low to no toxicity [47–49]. The human peripheral blood, particularly the erythrocytes has a negative surface charge which was attributed to

sialylated glycoproteins inside its membrane [50]. Since NCCs and functionalized NCCs had a negative particle surface charge too, this creates a repulsive electrostatic force that limits interaction with each other thus explaining the high haemocompatibility properties of NCCs and functionalized NCCs. NCCs' high biocompatibility allows them to function in blood without causing harm.

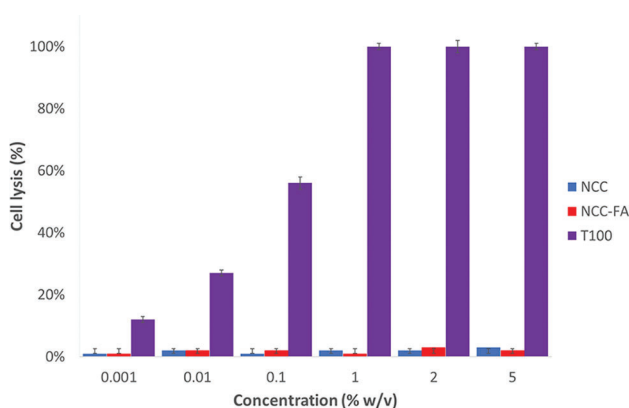


Figure 5: Percentage of red cell lysis in the solutions that contain different concentrations of NCC and NCC-FA relative to the positive control (100% red cell lysis in the solution that contains 1% w/v Triton \times 100) after 5 h of incubation at 37°C. Data are the mean \pm SD of at least three independent experiments

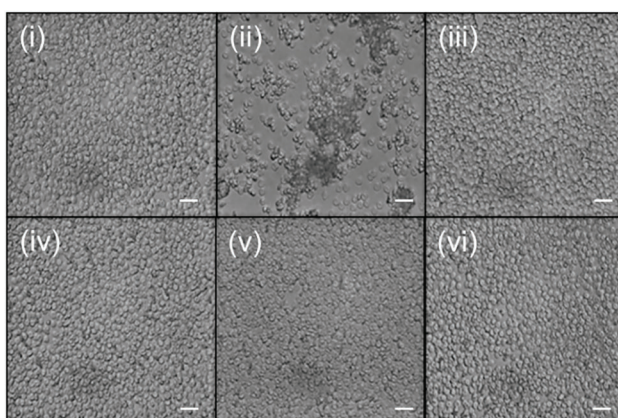


Figure 6: Representative photomicrographs showing erythrocytes samples incubated for 2 h and at 37°C with (i) negative control (ii) positive control (iii) 1% w/v NCC (iv) 5% w/v NCC (v) 1% w/v NCC-FA (vi) 5% w/v NCC-FA, $n = 3$, 100 \times magnification. Bar: 10 μ m

Evaluating cell proliferation and viability is a common practice in assessing the *in vitro* cytotoxicity of a substance, whether through direct or indirect contact. Methods that measure cellular growth, such as cell counting or confluency evaluation, are generally more sensitive and precise compared to approaches that involve placing test materials directly in cell cultures to determine the zone of growth inhibition [51]. The toxicity of cell lines can be attributed to various factors, including the presence of nanomaterials. Direct contact between different nanoparticles and cells can lead to cytotoxic effects within mitochondria. One commonly employed *in vitro* assay to assess mitochondrial damage caused by nanoparticles is the quantification and measurement of reductase/dehydrogenase enzyme activity within viable mitochondria [52,53]. The MTT assay is a widely utilized method for assessing cytotoxicity, which involves measuring the conversion of tetrazolium salt to formazan by viable cells. The resulting formazan product is then

detected through colorimetric analysis, and the quantity of formazan produced correlates directly with the number of viable cells present.

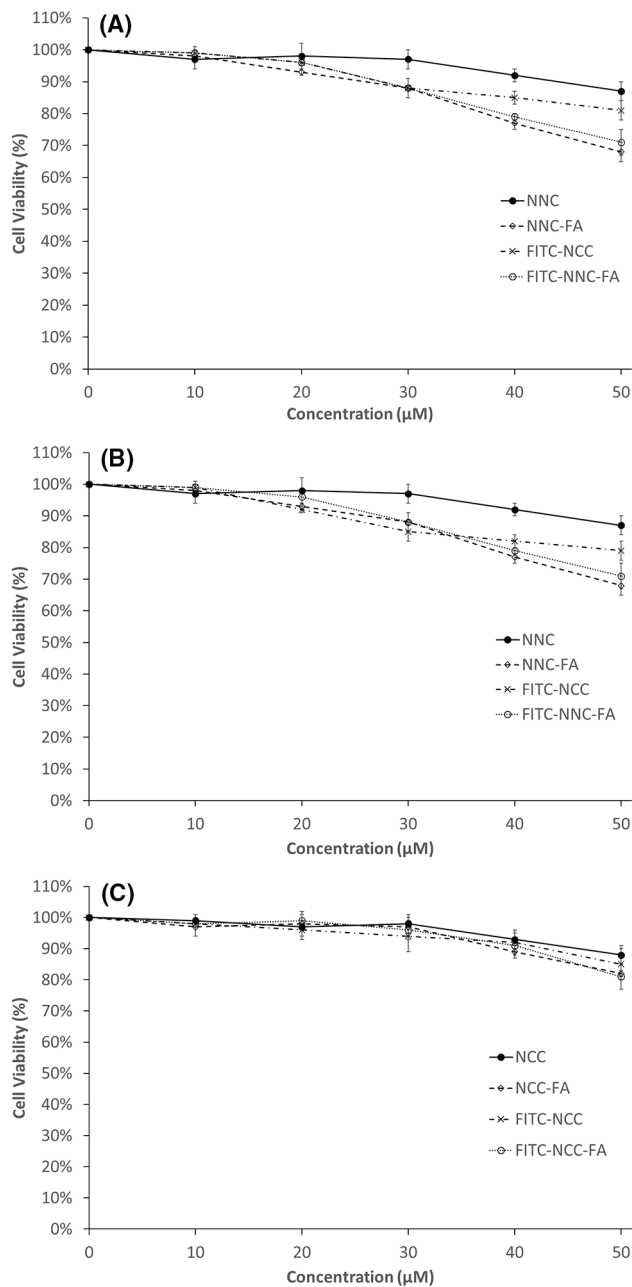


Figure 7: Percentage of cell viability (%) after 24 h treatment with NCC, NCC-FA, FITC-NCC and FITC-NCC-FA at different concentration. (A) CCD-18Co; (B) HT-29; (C) SW-620. Data are the mean \pm SD of at least three independent experiments

The cell toxicity test for NCC, NCC-FA, FITC-NCC and FITC-NCC-FA was shown in Fig. 7. NCCs did not show any significant effect on all three cell lines at low concentration but showed slight inhibition (87%–93%) at higher concentrations ($\geq 40 \mu\text{M}$). Meanwhile, NCC-FA, FITC-NCC and FITC-NCC-FA did not cause any significant effect on all three cell lines at lower concentrations ($\leq 20 \mu\text{M}$). At higher

concentrations ($\geq 30 \mu\text{M}$), both functionalized NCCs exhibit a higher inhibition rate at 68%–88% for both HT-29 and SW-620 cells. However, functionalized NCCs did not show such inhibition on CCD-18Co cells which remained at a higher cell viability rate of 81%–97%. Both HT-29 and SW-620 are colorectal cancer cell lines and folate receptors are only highly expressed on cancerous cells [54]. Since CCD-18Co is a noncancerous colorectal cell, it does not have high expression of folate receptors. This means NCC-FA and FITC-NCC-FA are readily bound to HT-29 and SW-620 cells via folate receptors. At higher concentrations, such binding can also cause cell viability inhibition on folate receptor positive cancerous cells. Such selective inhibition properties of the functionalized NCCs make it a suitable drug delivery system that actively targets folate receptor positive cancer tumors like colorectal cancer while leaving healthy cells relatively unaffected.

Nanoparticles can have a range of properties that contribute to their biocompatibility, depending on their composition, size, surface charge, and surface coating. Nanoparticles are typically less than 100 nanometers in diameter, which is smaller than many biological structures. This small size allows nanoparticles to penetrate tissues and cells more easily and reduces the likelihood of triggering immune responses [55]. TEM and particle size distribution showed that NCCs and FA-functionalized NCC are in the ideal size. The electrical charge on the surface of nanoparticles plays a crucial role in their interactions with biological tissues and cells. Nanoparticles that possess a neutral or slightly negative charge are typically considered more biocompatible compared to those with a significantly positive charge [56]. Nanoparticles must not be toxic to the biological environment to be considered biocompatible. They must not cause any harmful effects, such as cell death, tissue damage or immune responses. Results from ζ -potentials explain the high biocompatibility of NCCs and FA-functionalized NCCs with human peripheral blood and colon fibroblast cell lines. Although not tested in this study, biodegradability of the nanoparticles is also important. This can reduce the risk of long-term accumulation in the body and improve biocompatibility. NCCs are well known for their biodegradability [57]. On top of all the properties above, nanoparticle stability is crucial to ensure the integrity of the drug carrier during circulation and delivery. Factors such as pH, ionic strength can improve stability and prolong circulation time and increase the chances of successful tumor accumulation and drug release. Cellulose is known for its stability which makes it a promising biomaterial for biomedical applications [58]. Overall, both NCCs and FA-functionalized NCCs were shown in this study to fulfil all of the criteria mentioned above.

4 Conclusions

With the advancement of nanotechnology, biomass-based natural polymers are being discovered to be utilized in the biomedical field. Agricultural residues derived NCCs rendered morphology, biology and chemical properties that make it to be suitable as a drug carrier system. The successful FA-functionalized NCCs were observed with the presence of rod-shaped nanocrystallites with a width of 4–32 nm and length of 20–100 nm. The binding potential of FA conjugated NCC was first tested on HT-29 and SW-620 cell lines. FA-functionalized NCCs show an extremely high affinity towards FA. This particular property enables it to target folate receptor positive cancer cells with high efficiency. Investigations have also shown NCCs and FA-functionalized NCCs to have high biocompatibility. This makes them promising materials to be used for drug carrier systems on targeting cancer tumours or even diagnostic bioimaging agents for cancer detection.

Acknowledgement: None.

Funding Statement: This research was funded by Ministry of Higher Education (MOHE), Malaysia-Prototype Development Research Grant Scheme, Grant Number PRGS/1/2020/STG05/UM/02/1.

Author Contributions: Conceptualization, T.H.T. and W.A.Y.; Investigation, T.H.T.; Writing—original draft preparation, T.H.T.; Writing—review and editing, T.H.T., H.V.L., N.M.H., M.Z.F.; Visualization, T.H.T., H.V.L., N.M.H.; Supervision, H.V.L., W.A.Y., N.M.H.; Funding acquisition, H.V.L., M.Z.F. All authors have read and agreed to the published version of the manuscript.

Availability of Data and Materials: Data available on request from the authors. The data that support the findings of this study are available from the corresponding authors, (Hwei Voon Lee, Mochamad Zakki Fahmi), upon reasonable request.

Conflicts of Interest: The authors declare that they have no conflicts of interest to report regarding the present study.

References

1. Trache, D. (2018). Nanocellulose as a promising sustainable material for biomedical applications. *AIMS Materials Science*, 5(2), 201–205.
2. Yuce-Erarslan, E., Domb, A. A. J., Kasem, H., Uversky, V. N., Coskuner-Weber, O. (2023). Intrinsically disordered synthetic polymers in biomedical applications. *Polymers*, 15(10), 2406.
3. Alaswad, S. O., Mahmoud, A. S., Arunachalam, P. (2022). Recent advances in biodegradable polymers and their biological applications: A brief review. *Polymers*, 14(22), 4924.
4. Santolini, E., Bovo, M., Barbaresi, A., Torreggiani, D., Tassinari, P. (2021). Turning agricultural wastes into biomaterials: Assessing the sustainability of scenarios of circular valorization of corn cob in a life-cycle perspective. *Applied Sciences*, 11(14), 6281.
5. Zamri, M. F. M. A., Bahru, R., Amin, R., Aslam Khan, M. U., Razak, S. I. A. et al. (2021). Waste to health: A review of waste derived materials for tissue engineering. *Journal of Cleaner Production*, 290(16), 125792.
6. Elkodous, M. A., El-Husseiny, H. M., El-Sayyad, G. S., Hashem, A. H., Doghish, A. S. et al. (2021). Recent advances in waste-recycled nanomaterials for biomedical applications: Waste-to-wealth. *Nanotechnology Reviews*, 10(1), 1662–1739.
7. Jiang, G., Wang, G., Zhu, Y., Cheng, W., Cao, K. et al. (2022). A scalable bacterial cellulose ionogel for multisensory electronic skin. *Research*, 2022(11), 9814767.
8. Carter, N., Grant, I., Dewey, M., Bourque, M., Neivandt, D. (2021). Production and characterization of cellulose nanofiber slurries and sheets for biomedical applications. *Frontiers in Nanotechnology*, 3, 729743.
9. Dong, S., Cho, H. J., Lee, Y. W., Roman, M. (2014). Synthesis and cellular uptake of folic acid-conjugated cellulose nanocrystals for cancer targeting. *Biomacromolecules*, 15(5), 1560–1567.
10. Deepa, B., Abraham, E., Cordeiro, N., Mozetic, M., Mathew, A. P. et al. (2015). Utilization of various lignocellulosic biomass for the production of nanocellulose: A comparative study. *Cellulose*, 22(2), 1075–1090.
11. de Souza Lima, M. M., Borsali, R. (2004). Rodlike cellulose microcrystals: Structure, properties, and applications. *Macromolecular Rapid Communications*, 25(7), 771–787.
12. Chandel, N., Jain, K., Jain, A., Raj, T., Patel, A. K. et al. (2023). The versatile world of cellulose-based materials in healthcare: From production to applications. *Industrial Crops and Products*, 201(10), 116929.
13. Miyashiro, D., Hamano, R., Umemura (2020). A review of applications using mixed materials of cellulose, nanocellulose and carbon nanotubes. *Nanomaterials*, 10, 186.
14. Bacakova, L., Pajorova, J., Tomkova, M., Matejka, R., Broz, A. et al. (2020). Applications of nanocellulose/nanocarbon composites: Focus on biotechnology and medicine. *Nanomaterials*, 10(2), 196.
15. Kyriakides, T. R., Raj, A., Tseng, T. H., Xiao, H., Nguyen, R. et al. (2021). Biocompatibility of nanomaterials and their immunological properties. *Biomedical Materials*, 16(4), 042005.
16. Xinchun, Y., Jing, T., Jiaoqiong, G. (2023). Lipid-based nanoparticles via nose-to-brain delivery: A mini review. *Frontiers in Cell Development Biology*, 11, 1214450.
17. Salahpour Anarjan, F. (2019). Active targeting drug delivery nanocarriers: Ligands. *Nano-Structures & Nano-Objects*, 19, 100370.

18. Al-Thiabat, M. G., Saqallah, F. G., Gazzali, A. M., Mohtar, N., Yap, B. K. et al. (2021). Heterocyclic substitutions greatly improve affinity and stability of folic acid towards FR α . an in silico insight. *Molecules*, 26(4), 1079.
19. Hartmann, L. C., Keeney, G. L., Lingle, W. L., Christianson, T. J., Varghese, B. et al. (2007). Folate receptor overexpression is associated with poor outcome in breast cancer. *International Journal of Cancer*, 121(5), 938–942.
20. Dainty, L. A., Risinger, J. I., Morrison, C., Chandramouli, G. V., Bidus, M. A. et al. (2007). Overexpression of folate binding protein and mesothelin are associated with uterine serous carcinoma. *Gynecology Oncology*, 105(3), 563–570.
21. Toffoli, G., Cernigoi, C., Russo, A., Gallo, A., Bagnoli, M. et al. (1997). Overexpression of folate binding protein in ovarian cancers. *International Journal of Cancer*, 74(2), 193–198.
22. Weitman, S. D., Frazier, K. M., Kamen, B. A. (1994). The folate receptor in central nervous system malignancies of childhood. *Journal of Neurooncology*, 21(2), 107–112.
23. Nawaz, F. Z., Kipreos, E. T. (2022). Emerging roles for folate receptor FOLR1 in signaling and cancer. *Trends in Endocrinology & Metabolism*, 33(3), 159–174.
24. Yu, Y., Wang, J., Kaul, S. C., Wadhwa, R., Miyako, E. (2019). Folic acid receptor-mediated targeting enhances the cytotoxicity, efficacy, and selectivity of *Withania somnifera* leaf extract: *In vitro* and *in vivo* evidence. *Frontiers in Oncology*, 9, 602.
25. Chen, Y. W., Tan, T. H., Lee, H. V., Abd Hamid, S. B. (2017). Easy fabrication of highly thermal-stable cellulose nanocrystals using Cr(NO₃)₃ catalytic hydrolysis system: A feasibility study from macro- to nano-dimensions. *Materials*, 10(1), 42.
26. Yahya, M., Chen, Y. W., Lee, H. V., Hassan, W. H. W. (2018). Reuse of selected lignocellulosic and processed biomasses as sustainable sources for the fabrication of nanocellulose via Ni(II)-catalyzed hydrolysis approach: A comparative study. *Journal of Polymers and the Environment*, 26(7), 2825–2844.
27. Chen, Y. W., Lee, H. V. (2018). Revalorization of selected municipal solid wastes as new precursors of green nanocellulose via a novel one-pot isolation system: A source perspective. *International Journal of Biological Macromolecules*, 107(1), 78–92.
28. Sirviö, J. A., Visanko, M., Laitinen, O., Ämmälä, A., Liimatainen, H. (2016). Amino-modified cellulose nanocrystals with adjustable hydrophobicity from combined regioselective oxidation and reductive amination. *Carbohydrate Polymers*, 136, 581–587.
29. Salari, M., Bitounis, D., Bhattacharya, K., Pyrgiotakis, G., Zhang, Z. et al. (2019). Development & characterization of fluorescently tagged nanocellulose for nanotoxicological studies. *Environmental Science: Nano*, 6(5), 1516–1526.
30. Gausterer, J. C., Schübler, C., Gabor, F. (2021). The impact of calcium phosphate on FITC-BSA loading of sonochemically prepared PLGA nanoparticles for inner ear drug delivery elucidated by two different fluorimetric quantification methods. *Ultrasonics Sonochemistry*, 79(12), 105783.
31. Mahmoud, K. A., Mena, J. A., Male, K. B., Hrapovic, S., Kamen, A. et al. (2010). Effect of surface charge on the cellular uptake and cytotoxicity of fluorescent labeled cellulose nanocrystals. *ACS Applied Materials & Interfaces*, 2(10), 2924–2932.
32. Soleymani, J., Hasanzadeh, M., Somi, M. H., Jouyban, A. (2020). Differentiation and targeting of HT 29 cancer cells based on folate bioreceptor using cysteamine functionalized gold nano-leaf. *Material Science Engineering C*, 107, 110320.
33. Smith-Jones, P. M., Pandit-Taskar, N., Cao, W., O'Donoghue, J., Philips, M. D. et al. (2008). Preclinical radioimmunotargeting of folate receptor alpha using the monoclonal antibody conjugate DOTA-MORAb-003. *Nuclear Medicine Biology*, 35(3), 343–351.
34. Tsatsakis, A., Stratidakis, A. K., Goryachaya, A. V., Tzatzarakis, M. N., Stivaktakis, P. D. et al. (2019). *In vitro* blood compatibility and *in vitro* cytotoxicity of amphiphilic poly-N-vinylpyrrolidone nanoparticles. *Food and Chemical Toxicology*, 127, 42–52.
35. Jiao, L., Ma, J., Dai, H. (2015). Preparation and characterization of self-reinforced antibacterial and oil-resistant paper using a NaOH/Urea/ZnO solution. *PLoS One*, 10(10), e0140603.
36. Lex, A., Trimmel, G., Kern, W., Stelzer, F. (2006). Photosensitive polynorborene containing the benzyl thiocyanate group—synthesis and patterning. *Journal of Molecular Catalysis A: Chemical*, 254(1), 174–179.

37. Mohapatra, S., Mallick, S. K., Maiti, T. K., Ghosh, S. K., Pramanik, P. (2007). Synthesis of highly stable folic acid conjugated magnetite nanoparticles for targeting cancer cells. *Nanotechnology*, 18(38), 385102.
38. Colino, C. I., Lanao, J. M., Gutierrez-Millan, C. (2020). Targeting of hepatic macrophages by therapeutic nanoparticles. *Frontiers in Immunology*, 11, 218.
39. Hashizume, H., Baluk, P., Morikawa, S., McLean, J. W., Thurston, G. et al. (2000). Openings between defective endothelial cells explain tumor vessel leakiness. *American Journal of Pathology*, 156(4), 1363–1380.
40. Owens, D. E., Peppas, N. A. (2006). Opsonization, biodistribution, and pharmacokinetics of polymeric nanoparticles. *International Journal of Pharmaceutics*, 307(1), 93–102.
41. Lacerda, L., Herrero, M. A., Venner, K., Bianco, A., Prato, M. et al. (2008). Carbon-nanotube shape and individualization critical for renal excretion. *Small*, 4(8), 1130–1132.
42. Beyene, D., Chae, M., Dai, J., Danumah, C., Tosto, F. et al. (2018). Characterization of cellulase-treated fibers and resulting cellulose nanocrystals generated through acid hydrolysis. *Materials*, 11(8), 1272.
43. Prathapan, R., Thapa, R., Garnier, G., Tabor, R. F. (2016). Modulating the zeta potential of cellulose nanocrystals using salts and surfactants. *Colloids and Surfaces A: Physicochemical and Engineering Aspects*, 509, 11–18.
44. Sudimack, J., Lee, R. J. (2000). Targeted drug delivery via the folate receptor. *Advanced Drug Delivery Review*, 41(2), 147–162.
45. Destito, G., Yeh, R., Rae, C. S., Finn, M. G., Manchester, M. (2007). Folic acid-mediated targeting of cowpea mosaic virus particles to tumor cells. *Chemical Biology*, 14(10), 1152–1162.
46. Leamon, C. P., DePrince, R. B., Hendren, R. W. (1999). Folate-mediated drug delivery: Effect of alternative conjugation chemistry. *Journal of Drug Targeting*, 7(3), 157–169.
47. DeLoid, G. M., Cao, X., Molina, R. M., Silva, D. I., Bhattacharya, K. et al. (2019). Toxicological effects of ingested nanocellulose in *in vitro* intestinal epithelium and *in vivo* rat models. *Environmental Science: Nano*, 6(7), 2105–2115.
48. Pinto, F., Lourenço, A. F., Pedrosa, J. F. S., Gonçalves, L., Ventura, C. et al. (2022). Analysis of the *in vitro* toxicity of nanocelluloses in human lung cells as compared to multi-walled carbon nanotubes. *Nanomaterials*, 12(9), 1432.
49. Vital, N., Ventura, C., Kranendonk, M., Silva, M. J., Louro, H. (2022). Toxicological assessment of cellulose nanomaterials: Oral exposure. *Nanomaterials*, 12(19), 3375.
50. Fernandes, H. P., Cesar, C. L., Barjas-Castro Mde, L. (2011). Electrical properties of the red blood cell membrane and immunohematological investigation. *Revista Brasileira de Hematologia e Hemoterapia*, 33(4), 297–301.
51. Kamiloglu, S., Sari, G., Ozdal, T., Capanoglu, E. (2020). Guidelines for cell viability assays. *Food Frontiers*, 1(3), 332–349.
52. Ghasemi, M., Turnbull, T., Sebastian, S., Kempson, I. (2021). The MTT assay: Utility, limitations, pitfalls, and interpretation in bulk and single-cell analysis. *International Journal of Molecular Science*, 22(23), 12827.
53. Acin-Perez, R., Benincá, C., Shabane, B., Shirihai, O. S., Stiles, L. (2021). Utilization of human samples for assessment of mitochondrial bioenergetics: Gold standards, limitations, and future perspectives. *Life*, 11(9), 949.
54. Zwicke, G. L., Mansoori, G. A., Jeffery, C. J. (2012). Utilizing the folate receptor for active targeting of cancer nanotherapeutics. *Nano Reviews*, 3(1), 18496.
55. Kus-Liśkiewicz, M., Fickers, P., Ben Tahar, I. (2021). Biocompatibility and cytotoxicity of gold nanoparticles: Recent advances in methodologies and regulations. *International Journal of Molecular Science*, 22(20), 10952.
56. Frohlich, E. (2012). The role of surface charge in cellular uptake and cytotoxicity of medical nanoparticles. *International Journal of Nanomedicine*, 7, 5577–5591.
57. Zinge, C., Kandasubramanian, B. (2020). Nanocellulose based biodegradable polymers. *European Polymer Journal*, 133, 109758.
58. Ciolacu, D. E., Nicu, R., Ciolacu, F. (2020). Cellulose-based hydrogels as sustained drug-delivery systems. *Materials*, 13(22), 5270.